THE JOURNAL OF PHYSICAL CHEMISTRY LETTERS
A JOURNAL OF THE AMERICAN CHEMICAL SOCIETY

pubs.acs.org/JPCL

Letter

Ultrafast Extreme Ultraviolet Photoelectron Spectroscopy of Nonadiabatic Photodissociation of CS_2 from $^1B_2$ ($^1\Sigma_u^+$) State: Product Formation via an Intermediate Electronic State

Shutaro Karashima, Yoshi-Ichi Suzuki, and Toshinori Suzuki*

Cite This: *J. Phys. Chem. Lett.* 2021, 12, 3755−3761

Read Online

ACCESS | Metrics & More | Article Recommendations | Supporting Information

ABSTRACT: We studied nonadiabatic dissociation of CS_2 from the $^1B_2$ ($^1\Sigma_u^+$) state using ultrafast extreme ultraviolet photoelectron spectroscopy. A deep UV (200 nm) laser using the filamentation four-wave mixing method and an extreme UV (21.7 eV) laser using the high-order harmonic generation method were employed to achieve the pump−probe laser cross-correlation time of 48 fs. Spectra measured with a high signal-to-noise ratio revealed clear dynamical features of vibrational wave packet motion in the $^1B_2$ state; its electronic decay to lower electronic state(s) within 630 fs; and dissociation into $S(^1D_2)$, $S(^3P_J)$, and CS fragments within 300 fs. The results suggest that both singlet and triplet dissociation occur via intermediate electronic state(s) produced by electronic relaxation from the $^1B_2$ ($^1\Sigma_u^+$) state.

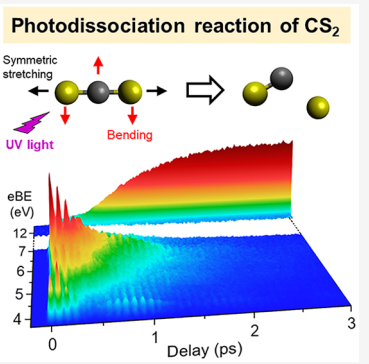

Photoexcited polyatomic molecules undergo multiple electronic relaxation processes such as internal conversion and intersystem crossing, which lead to formation of various reaction products. Understanding the mechanistic details of these complex electronic dynamics is one of the main research subjects in molecular reaction dynamics.[1,2] UV photodissociation of carbon disulfide from the $^1B_2$ ($^1\Sigma_u^+$) state is known to produce both singlet and triplet products (Figure 1)

$$CS_2(^1B_2(^1\Sigma_u^+)) \rightarrow CS(X^1\Sigma^+) + S(^1D_2) \quad (1a)$$

$$\rightarrow CS(X^1\Sigma^+) + S(^3P_J) \quad (1b)$$

Interestingly, the spin-forbidden channel (eq 1b) has a greater quantum yield than the spin-allowed channel (eq 1a).[3−10] This reaction has been studied using a plethora of experimental methods; however, the mechanism involved is yet to be understood.[3−25] In this Letter, we report time-resolved extreme UV (EUV) photoelectron spectroscopy (TRPES) with the pump−probe cross-correlation time of 48 fs, which was obtained by the combination of an ultrafast deep UV (6.2 eV; 200 nm) laser based on filamentation four-wave mixing (FFWM)[26−29] and an EUV (21.7 eV) laser based on high-order harmonic generation (HHG).[30−32] As discussed later, a high temporal resolution and signal-to-noise ratio are crucial for extraction of dynamical information such as the nuclear wave packet motions in the $^1B_2$ state, electronic relaxation from $^1B_2$ to intermediate electronic state(s), and subsequent dissociation into the singlet and triplet reaction products.

The UV photoabsorption spectrum of jet-cooled CS_2[34] and the spectrum of our DUV pump pulse are presented in Figure 2a. The $^1B_2$ potential energy surface has a minimum for a bent molecular geometry, while a relatively low barrier to linearity exists at around a photoexcitation energy of 6.1 eV (204 nm).[13,34,35] Therefore, the pump laser pulse creates a vibrational wave packet just above the barrier in the $^1B_2$ state. Figure 2b presents an overview of the TRPES results. The horizontal axis of this figure corresponds to the electron binding energy (eBE), given by the difference between the probe photon energy and the experimentally measured photoelectron kinetic energy (PKE). The negative bands seen at 10, 13, and 14.5 eV (indicated in purple) are due to the ground-state bleach (depopulation) induced by the pump pulses; the pump efficiency is estimated to be 0.7%. The photoemission signals associated with the reaction products start appearing from about 500 fs with high intensities; on the other hand, the photoemission signals from the photoexcited $^1B_2$ state of CS_2 in the eBE region lower than 10 eV are considerably weaker. In order to examine these weak signals, the spectra in the region enclosed by the white dashed box in Figure 2b are presented using a different color scheme in Figure 2c. The photoionization signal between 4 and 7 eV is due to the transition from $^1B_2$ to the cationic ground state

Received: March 17, 2021
Accepted: April 7, 2021

https://doi.org/10.1021/acs.jpclett.1c00864
J. Phys. Chem. Lett. 2021, 12, 3755−3761

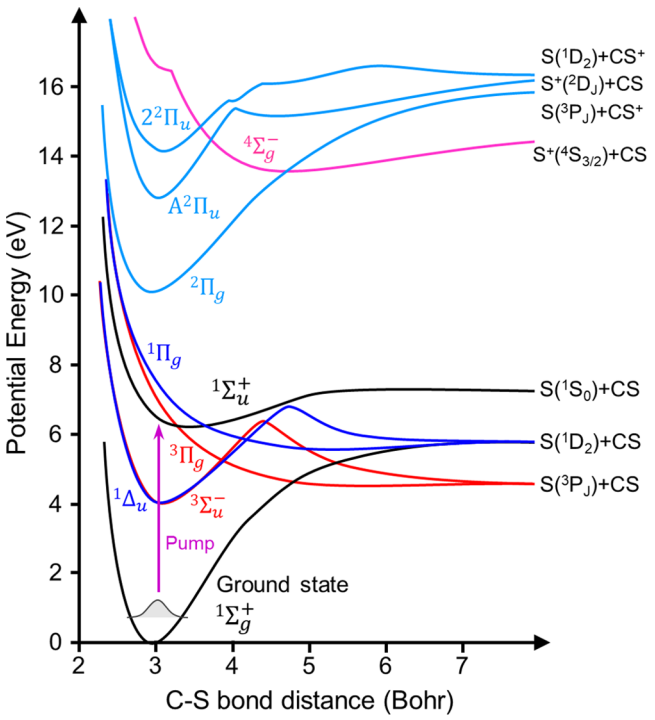

Figure 1. Schematic potential energy curves along the C−S bond distance.[33]

($^2\Pi_g$). The signal at 4 eV corresponds to ionization from the linear molecular geometry (the Franck−Condon region), and the signal at 7 eV is from the region of outer turning points for both bending and asymmetric stretching vibrations. It is noted that the appearance time of the intensity maximum in the 9.5−10 eV region is delayed with respect to that in the 4−7 eV region, indicating photoionization from intermediate electronic states populated by electronic relaxation from $^1B_2$, as previously discussed by Smith et al.[20]

Photoionization from the $^1B_2$ state and the intermediate electronic state(s) to higher cationic states also occurs, and the corresponding signals should appear in the eBE region higher than 10 eV; for example, a short-lived photoemission signal from $^1B_2$ is seen at 10.6 eV. Close examination of Figure 2b reveals a quantum beat signal due to vibrational wave packet motion in the $^1B_2$ state in the 11−12.5 eV region. It is important to consider these photoemission signals from the excited states of CS_2 in order to perform a reliable analysis of the time profiles of the reaction products, as discussed in detail later.

We first focus on the eBE region below 10 eV; Figure 3 shows representative time profiles for the photoelectron signals. The profiles are integrated signals in the eBE ranges of (a) 3.8−6.7 and (b) 7.0−9.8 eV. These profiles exhibit no signature of a vibrational quantum beat, as the signal was integrated for sufficiently wide eBE ranges, and they represent population decay. We performed least-squares fitting of these two profiles by assuming (a) mono- and (b) biexponential decay functions, and we obtained τ_1 and τ_2 values of 626 ± 14 and 299 ± 2 fs, respectively. τ_1 corresponds to the population decay time for the $^1B_2$ state, and τ_2 is the decay time for the lower electronic state populated by electronic relaxation from $^1B_2$. Because τ_2 is shorter than τ_1, the photoemission signal in the 7.0−9.8 eV region rises with τ_2 and decays with τ_1. The integrated profiles for narrower eBE ranges, shown in Figure 3c−e, clearly reveal vibrational quantum beats. A Fourier transform of these beat signals provides four frequencies, which correspond to vibrational energy spacings of 4.5, 44, 50, and 55 meV (36, 357, 401, and 440 cm^{-1}) for the $^1B_2$ state (see section S1 of the Supporting Information for details). In

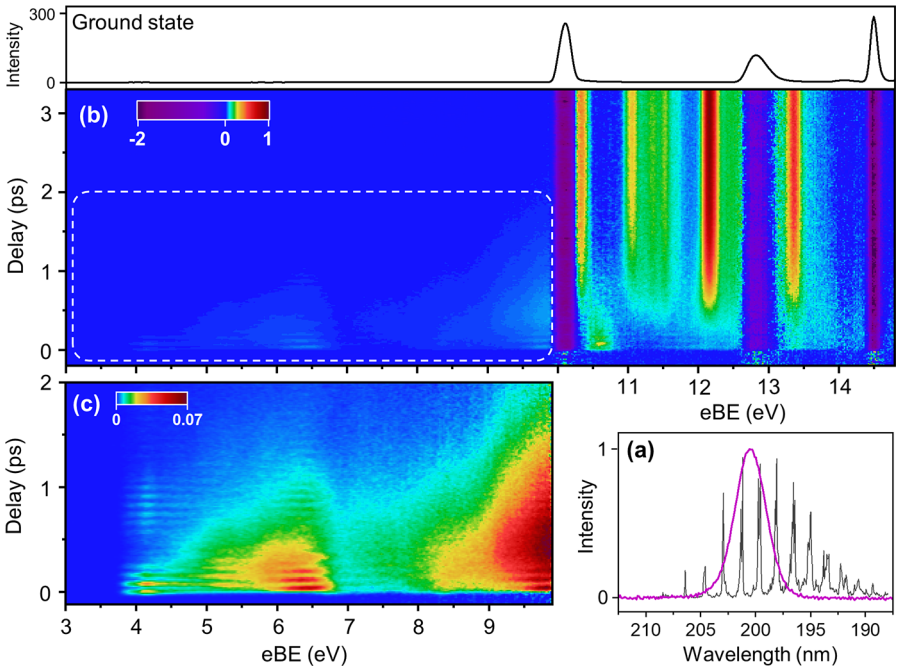

Figure 2. (a) Ultraviolet photoabsorption spectra of jet-cooled CS_2[34] (gray) and our pump pulses (purple). (b) Two-dimensional map of photoelectron spectra measured for jet-cooled CS_2 using 200 nm pump and 21.7 eV probe pulses. A static photoelectron spectrum of jet-cooled CS_2 is shown above the map. (c) Magnified view of the data enclosed in dashed box in panel b using a different color scheme to enhance the visibility.

https://doi.org/10.1021/acs.jpclett.1c00864
J. Phys. Chem. Lett. 2021, 12, 3755−3761

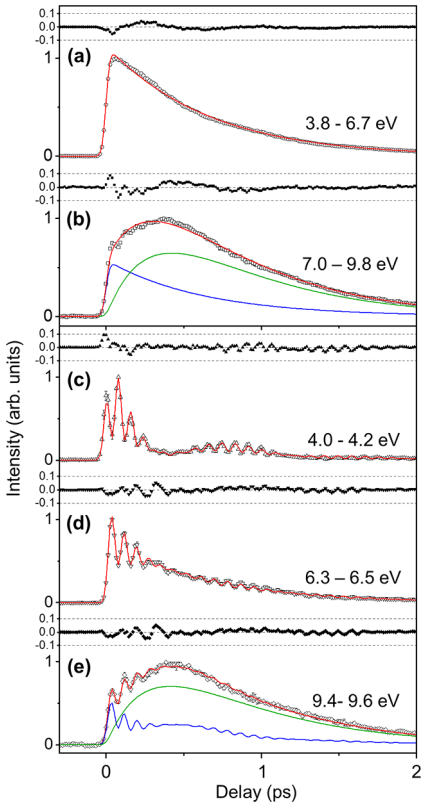

Figure 3. Time profiles of photoelectron intensity integrated over eBE ranges of (a) 3.8−6.7, (b) 7.0−9.8, (c) 4.0−4.2, (d) 6.3−6.5, and (e) 9.4−9.6 eV. Open symbols show experimental data, and solid lines are the best-fit profiles obtained using eq 5. Red, blue, and green lines represent the total intensity, $^1B_2$ state, and intermediate state(s), respectively. Error bars show the standard deviation. Black filled symbols show the residuals of the least-squares fitting. Because the curve fitting was performed by assuming only four principal beat frequencies, weak oscillatory features remain in the residuals.

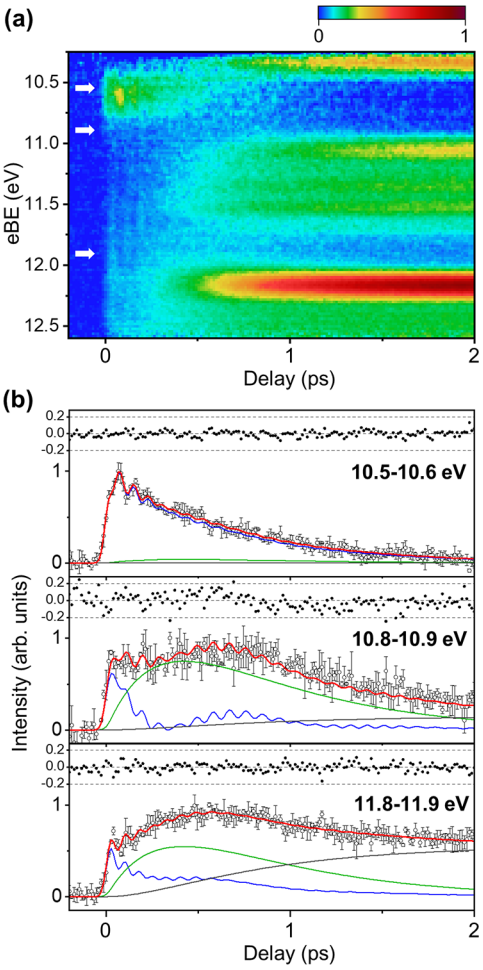

Figure 4. (a) Two-dimensional map of photoelectron spectra expanded in the region of 9.9−12.8 eV. (b) Time profiles of photoelectron intensity at selected eBE values indicated by arrows in panel a. Open symbols in the main panels show the experimental results, and the solid lines are the best-fit profiles obtained using eq 5. Red lines are curves of total intensity, and blue, green, and gray lines show the contribution of the $^1B_2$ state, intermediate state, and products, respectively. Error bars show the standard deviation. Filled symbols in the upper panels show the residuals.

previous time-resolved photoelectron imaging (TRPEI) experiments using deep UV pump and probe pulses, we observed additional higher frequencies;[17,18] however, they are not observed in the present study owing to the slightly narrower bandwidth of the pump pulse. The profile in the region of 9.4−9.6 eV shown in Figure 3e exhibits a quantum beat on top of a slowly varying signal, whose intensity exhibits a maximum at around 500 fs. The beating component in this time-profile is due to ionization from $^1B_2$, while the slowly varying component is due to ionization from lower electronic state(s). The solid lines in Figure 3 are the results of least-squares fitting using a kinetic model described later.

Next, we discuss the spectral features in the eBE region higher than 10 eV. As described earlier, excited-state photoemission signals also appear in this region. Figure 4a shows an expanded view of the two-dimensional map of photoelectron spectra. The vibrational quantum beat in the $^1B_2$ state can be seen near the time origin. Figure 4b shows the time profiles in the eBE regions of 10.5−10.6, 10.8−10.9, and 11.8−11.9 eV along with least-squares fits to estimate the contributions of the excited-state signal. The photoemission signal from the $^1B_2$ state is dominant in the decay profile at 10.5−10.6 eV, while signals from intermediate electronic states are seen in both the 10.8−10.9 and 11.8−11.9 eV regions.

Figure 5a shows a photoelectron spectrum of the products measured at delay times longer than 3 ps, in which the ground-state bleach was compensated for by addition of the EUV photoelectron spectrum of CS_2 measured with the same apparatus. The red and green ticks above the spectrum indicate the spectral assignments for the $S(^3P_J)$ and $S(^1D_2)$ photoemission bands.[36−38] From the intensities of these bands, we estimated the $S(^3P_J)/S(^1D_2)$ branching ratio to be 2.47 (see section S4 of the Supporting Information for details). We also estimated the vibrational state distribution for $CS(^1\Sigma^+)$ fragments from the photoelectron spectra of $CS(^1\Sigma^+)$ seen in Figure 5a using a Franck−Condon analysis; the Franck−Condon factors for the two ionization transitions to the $X\ ^2\Sigma^+$ and $A\ ^2\Pi$ states of CS^+ were evaluated using reported spectroscopic parameters for CS and CS^+ in refs 39−42, and the two bands were fitted using the common parameters for the $CS(^1\Sigma^+)$ state (see sections S2 and S3 of the Supporting Information for details). The analysis indicated that the population over the vibrational states of $CS(^1\Sigma^+)$ gradually declines with vibrational quantum number. Therefore, we approximated the distribution using the simple exponential function $\exp(-k \times \Delta E_{vib})$, where k is a constant and ΔE_{vib} is

https://doi.org/10.1021/acs.jpclett.1c00864
J. Phys. Chem. Lett. 2021, 12, 3755−3761

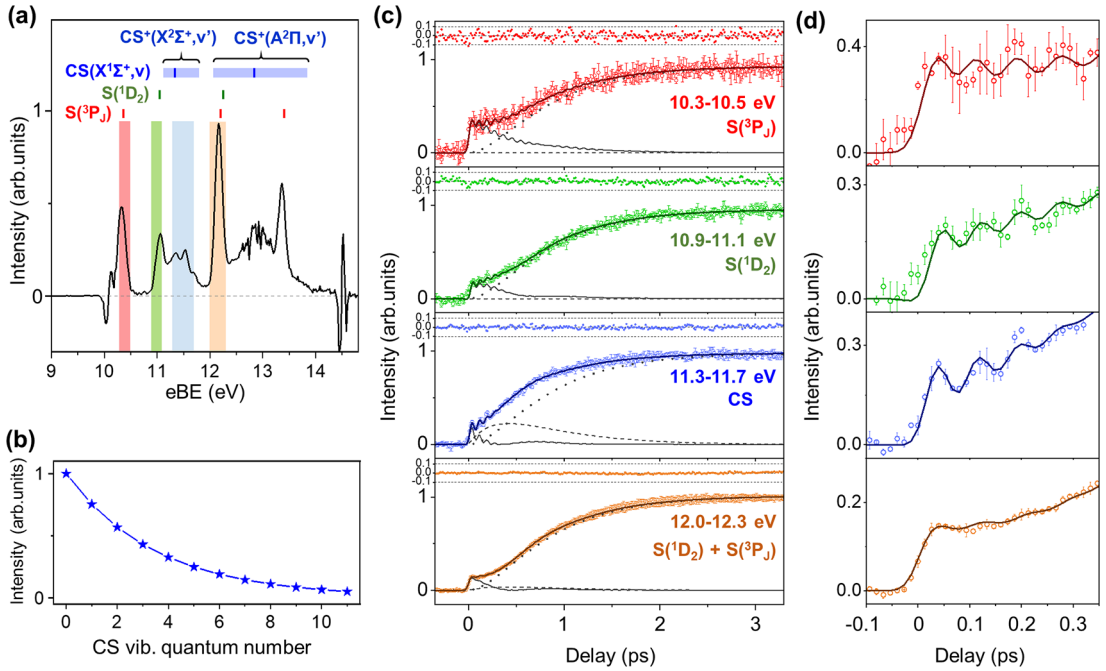

Figure 5. (a) Photoelectron spectra measured for delay times greater than 3 ps. Four colored bands indicate the eBE ranges for which the integrated intensity time profiles are examined in c and d. (b) Vibrational state distributions for CS fragments estimated from photoionization to X $^2\Sigma^+$ and A $^2\Pi$ states of CS^+. (c) Time profiles for photoelectron intensity at selected eBE ranges. Experimental results, total fitting curve, and residuals are plotted as colored open circles with error bars, solid lines, and closed circles, respectively. Solid, broken, and dotted gray lines indicate populations of $^1B_2$ state, intermediate state, and reaction product, respectively. (d) Enlarged views of time profiles shown in panel c.

the vibrational energy difference. The estimated CS vibrational distribution, shown in Figure 5b, is in reasonable agreement with the distribution at 210−216 nm for photodissociation of CS_2.[12] Considering energy partitioning into translational and rotational degrees of freedom, formation of CS ($v'' = 3$) is not expected for the $S(^1D_2)$ channel for 200 nm photodissociation. Then, if we assume that half of the CS product for $v'' = 0$−2 is produced by the $S(^1D_2)$ channel, the overall $S(^3P_J)/S(^1D_2)$ branching ratio is estimated to be 2.43, which agrees well with the aforementioned value of 2.47.

Figure 5c presents the photoelectron intensity profiles observed at the eBE positions for the atomic and molecular products. All of these profiles have a sufficiently high signal-to-noise ratio for detailed examination. As described earlier, the photoelectron signals observed for these eBE values immediately after UV photoexcitation involve contributions from the photoexcited $^1B_2$ state and a metastable electronic state of CS_2. In order to clarify this point, enlarged views of the rising edges of these signals are shown in Figure 5d; the vibrational quantum beats unambiguously represent the photoemission signal from the $^1B_2$ state. Thus, the photoelectron signal intensities for fragments were estimated by considering the following kinetic scheme:

$$\begin{array}{l} CS_2(^1B_2) \xrightarrow{\tau_S} CS_2(S) \xrightarrow{\tau_{Sd}} CS + S(^1D_2) \\ \qquad\quad \searrow^{\tau_T} \\ \qquad\quad CS_2(T) \xrightarrow{\tau_{Td}} CS + S(^3P_J) \end{array} \qquad \text{(A)}$$

where $CS_2(S)$ and $CS_2(T)$ indicate the singlet and triplet intermediate electronic states, respectively. From the aforementioned lifetime of the $^1B_2$ state (0.63 ps) and the triplet/singlet branching ratio (2.47), the time constants τ_S and τ_T are estimated to be 2.2 and 0.88 ps, respectively. Least-squares fitting of the time profiles for $S(^1D_2)$ and $S(^3P_J)$ indicated that the rise times of products τ_{Sd} (322 ± 23 fs) and τ_{Td} (358 ± 48 fs) agree with each other within experimental errors, and they are also indistinguishably similar to the decay time constant (299 ± 2 fs) for the intermediate state estimated from the photoemission time profile shown in Figure 3b,e (see section S5 of the Supporting Information for details). Thus, we simplified the reaction scheme by assuming $\tau_1 = (1/\tau_S + 1/\tau_T)^{-1}$, $\tau_2 = \tau_{Sd} = \tau_{Td}$ as follows:

$$CS_2(^1B_2) \xrightarrow{\tau_1} \text{Intermediate state} \xrightarrow{\tau_2} \text{Products} \qquad \text{(B)}$$

This does not immediately imply that the singlet and triplet products are formed from a single intermediate electronic state but that, even if there are multiple singlet and triplet intermediate states, their temporal behaviors are indistinguishably similar. The analytical solutions for this scheme are expressed as

$$\begin{cases} [^1B_2] = \exp\left(-\dfrac{t}{\tau_1}\right) & (1) \\ [\text{IS}] = \dfrac{\tau_2}{\tau_2 - \tau_1}\left\{\exp\left(-\dfrac{t}{\tau_2}\right) - \exp\left(-\dfrac{t}{\tau_1}\right)\right\} & (2) \\ [\text{Product}] = 1 + \dfrac{1}{\tau_2 - \tau_1}\left\{\tau_1\exp\left(-\dfrac{t}{\tau_1}\right) - \tau_2\exp\left(-\dfrac{t}{\tau_2}\right)\right\} & (3) \end{cases}$$

where $[^1B_2]$, [IS], and [Products] are the populations of $^1B_2$, intermediate electronic state, and reaction products, respectively. The initial population in $^1B_2$ was assumed to be unity. We considered the vibrational quantum beats in the $^1B_2$ state using the following functional form:

https://doi.org/10.1021/acs.jpclett.1c00864
J. Phys. Chem. Lett. 2021, 12, 3755−3761

$$[\mathrm{Osc}_i] = \cos\left(\frac{2\pi t}{T_i} - \phi_i\right)\exp\left(-\frac{t}{\tau_i}\right) \quad (4)$$

where τ_i is the damping time of quantum beat; T_i and ϕ_i are the vibrational period and the initial phase, respectively. T_i has been determined using Fourier transformation as described earlier. Thus, the functional form for the least-squares fitting was

$$I(t) = \left\{\left(c_1[^1B_2] + c_2[\mathrm{IS}] + c_3[\mathrm{Products}] + \sum_{i=4}^{7} c_i[\mathrm{Osc}_i]\right)U(t)\right\} \otimes G(t) \quad (5)$$

where c_i are the expansion coefficients; $U(t)$ is a unit step function, and $G(t)$ is a Gaussian-shaped cross-correlation function for the pump and probe laser pulses. The time constants determined by the least-squares fitting are listed in Table 1, and simulated curves are shown in Figures 3, 4b, and 5c,d.

Table 1. Best Fit Parameters for Time Profiles of Excited States

excited states			
		ΔE^a	
component	decay time (fs)	(cm^{-1})	(meV)
$^1B_2$	626 ± 14		
Intermediate	299 ± 2		
$\nu_2 - \nu_1$ [b]	335 ± 15	36	4.5
$2\nu_1 - \nu_2$ [b]	774 ± 143	357	44
ν_1 [b]	723 ± 100	401	50
ν_2 [b]	162 ± 16	440	55

[a]Quantum beat frequency expressed in the form of vibrational energy gap. [b]Refs 17, 18, 34, and 35.

Previously, TRPEI study by Horio et al. suggested that $S(^1D_2)$ reaction products appear after a certain latency time,[19] which suggests the presence of an intermediate state for the singlet dissociation channel. In this sense, our conclusion is consistent with that of Horio et al. Minns and colleagues proposed a slightly different kinetic model, which assumes that the singlet reaction products are generated directly from $^1B_2$; however, we found that the experimental data presented here cannot be well-explained with their model.[20,21] They measured similar time profiles with the cross-correlation time of 180 fs and performed the analysis without considering molecular signals. As presented in section S6 of the Supporting Information, when the experimental data shown in Figure 5c are convoluted with a Gaussian function with a full width at half-maximum (fwhm) of 180 fs, the time profiles become much smoother and the position of initial signal rise become elusive. Thus, we believe the difference between the two studies largely originates from the low temporal resolution and the lack of consideration of molecular signals.[20,21]

In conclusion, we performed ultrafast EUV photoelectron spectroscopy on CS_2 with the pump−probe cross-correlation time of 48 fs using FFWM and HHG light sources. The $^1B_2$ state exhibited a vibrational quantum beat and decayed in 630 fs to populate metastable electronic state(s). The metastable state decays into singlet and triplet products with an indistinguishably similar time constant of 300 fs. The triplet/singlet branching ratio is estimated to be about 2.5, and the vibrational population of CS declines with vibrational quantum number. In the present study, we employed a magnetic bottle time-of-flight electron spectrometer and considered only the electron kinetic energy distribution and its time-evolution. Further information could be obtained from photoelectron angular distribution measured using TRPEI with an EUV laser.

METHODS

The experimental apparatus is described in more detail elsewhere.[29] We employed a one-box Ti:sapphire laser (Coherent Astrella, 35 fs, 800 nm, 6 mJ) as a driving laser. Pump pulses with a wavelength of 200 nm (30 nJ) were generated using FFWM in Ar with the fundamental (800 nm, 0.5 mJ) and the second harmonic (400 nm, 0.3 mJ) of the Ti:sapphire laser. The 200 nm pulses were separated from other harmonics using multilayer mirrors and gently focused into the photoionization chamber. The probe pulse was generated using an HHG process in Kr gas. The second harmonic (0.29 mJ) was focused into a Teflon tube filled with Kr gas at a pressure of 43 Torr to generate high harmonics, and a single harmonic (21.7 eV) was separated using a time-preserving monochromator. The probe pulses were focused into the photoionization chamber with a toroidal mirror. Carbon disulfide was seeded in He career gas (8%) and injected into a photoionization chamber through a pinhole (⌀ 0.1 mm) at a stagnation pressure of 0.08 MPa at room temperature. The photoionization chamber was evacuated with a turbo molecular pump (1380 L/s) to maintain its pressure at 4.0×10^{-5} Torr. The PKE distribution was measured using a magnetic bottle time-of-flight electron spectrometer with a 1.3 m flight path length.[43] The photoelectrons were detected using a microchannel plate, and the signal was preamplified and integrated using an A/D converter. The energy resolution was estimated to be 120 meV. The pump−probe cross-correlation time was estimated to be 48 fs using nonresonant ionization of Xe.

ASSOCIATED CONTENT

Supporting Information

The Supporting Information is available free of charge at https://pubs.acs.org/doi/10.1021/acs.jpclett.1c00864.

S1, Fourier transform analysis of vibrational quantum beats in $^1B_2$ state; S2, Franck−Condon analysis of photoelectron spectrum of CS; S3, fitting analysis of photoelectron spectra; S4, branching ratio into singlet and triplet products; S5, least-squares fitting of photoelectron intensity time profiles of $S(^1D_2)$ and $S(^3P_J)$ using scheme A; intensity time profiles of reaction products convoluted with a Gaussian function with a full width at half-maximum of 180 fs (PDF)

AUTHOR INFORMATION

Corresponding Author

Toshinori Suzuki − *Department of Chemistry, Graduate School of Science, Kyoto University, Kyoto 606-8502, Japan;* orcid.org/0000-0002-4603-9168; Email: suzuki@kuchem.kyoto-u.ac.jp

Authors

Shutaro Karashima − *Department of Chemistry, Graduate School of Science, Kyoto University, Kyoto 606-8502, Japan*

Yoshi-Ichi Suzuki − *School of Medical Technology, Health Sciences University of Hokkaido, Ishikari, Hokkaido 061-0293, Japan*

Complete contact information is available at: https://pubs.acs.org/10.1021/acs.jpclett.1c00864

Notes

The authors declare no competing financial interest.

■ ACKNOWLEDGMENTS

This work was supported by JSPS KAKENHI Grant No. 15H05753 and Mitsubishi Foundation. We thank T. Horio for helpful discussions.

■ REFERENCES

(1) Domcke, W.; Yarkony, D. R.; Koppel, H. *Conical Intersections: Electronic Structure, Dynamics & Spectroscopy*; World Scientific Publishing Co. Pte. Ltd.: Singapore, 2004; Vol. *15*.

(2) Domcke, W.; Yarkony, D. R.; Koppel, H. *Conical Intersections: Theory, Computation and Experiment*; World Scientific Publishing Co. Pte. Ltd.: Singapore, 2011; Vol. *17*.

(3) Waller, I. M.; Hepburn, J. W. Photofragment Spectroscopy of CS_2 at 193 nm - Direct Resolution of Singlet and Triplet Channels. *J. Chem. Phys.* **1987**, *87*, 3261−3268.

(4) Starrs, C.; Jego, M. N.; Mank, A.; Hepburn, J. W. Mode Specific Photodissociation of the $^1B_2$ State of CS_2. *J. Phys. Chem.* **1992**, *96*, 6526−6529.

(5) Mank, A.; Starrs, C.; Jego, M. N.; Hepburn, J. W. A Detailed Study of the Predissociation Dynamics of the $^1B_2(^1\sum_u^+)$ State of CS_2. *J. Chem. Phys.* **1996**, *104*, 3609−3619.

(6) Tzeng, W. B.; Yin, H. M.; Leung, W. Y.; Luo, J. Y.; Nourbakhsh, S.; Flesch, G. D.; Ng, C. Y. A 193 nm Laser Photofragmentation Time-of-Flight Mass-Spectrometric Study of CS_2 and CS_2 Clusters. *J. Chem. Phys.* **1988**, *88*, 1658−1669.

(7) McGivern, W. S.; Sorkhabi, O.; Rizvi, A. H.; Suits, A. G.; North, S. W. Photofragment Translational Spectroscopy with State-Selective "Universal Detection": The Ultraviolet Photodissociation of CS_2. *J. Chem. Phys.* **2000**, *112*, 5301−5307.

(8) Kitsopoulos, T. N.; Gebhardt, C. R.; Rakitzis, T. P. Photodissociation Study of CS_2 at 193 nm Using Slice Imaging. *J. Chem. Phys.* **2001**, *115*, 9727−9732.

(9) Xu, D. D.; Huang, J. H.; Jackson, W. M. Reinvestigation of CS_2 Dissociation at 193 nm by Means of Product State-Selective Vacuum Ultraviolet Laser Ionization and Velocity Imaging. *J. Chem. Phys.* **2004**, *120*, 3051−3054.

(10) Brouard, M.; Campbell, E. K.; Cireasa, R.; Johnsen, A. J.; Yuen, W. H. The Ultraviolet Photodissociation of CS_2: The $S(^1D_2)$ Channel. *J. Chem. Phys.* **2012**, *136*, No. 044310.

(11) Yang, S. C.; Freedman, A.; Kawasaki, M.; Bersohn, R. Energy Distribution of the Fragments Produced by Photodissociation of CS_2 at 193 nm. *J. Chem. Phys.* **1980**, *72*, 4058−4062.

(12) Chen, J.; Guo, Y.; Zhou, X. G.; Shi, Y.; Liu, S. L.; Ma, X. X. K-Dependent Predissociation Dynamics of CS_2 in the 210−216 nm Region. *J. Phys. Chem. A* **2007**, *111*, 5382−5387.

(13) Farmanara, P.; Stert, V.; Radloff, W. Ultrafast Predissociation and Coherent Phenomena in CS_2 Excited by Femtosecond Laser Pulses at 194−207 nm. *J. Chem. Phys.* **1999**, *111*, 5338−5343.

(14) Townsend, D.; Satzger, H.; Ejdrup, T.; Lee, A. M. D.; Stapelfeldt, H.; Stolow, A. $^1B_2(^1\Sigma_u^+)$ Excited State Decay Dynamics in CS_2. *J. Chem. Phys.* **2006**, *125*, 234302.

(15) Bisgaard, C. Z.; Clarkin, O. J.; Wu, G. R.; Lee, A. M. D.; Gessner, O.; Hayden, C. C.; Stolow, A. Time-Resolved Molecular Frame Dynamics of Fixed-in-Space CS_2 Molecules. *Science* **2009**, *323*, 1464−1468.

(16) Hockett, P.; Bisgaard, C. Z.; Clarkin, O. J.; Stolow, A. Time-Resolved Imaging of Purely Valence-Electron Dynamics During a Chemical Reaction. *Nat. Phys.* **2011**, *7*, 612−615.

(17) Fuji, T.; Suzuki, Y. I.; Horio, T.; Suzuki, T. Excited-State Dynamics of CS_2 Studied by Photoelectron Imaging with a Time Resolution of 22 fs. *Chem. - Asian J.* **2011**, *6*, 3028−3034.

(18) Spesyvtsev, R.; Horio, T.; Suzuki, Y. I.; Suzuki, T. Observation of the Wavepacket Dynamics on the $^1B_2(^1\Sigma_u^+)$ State of CS_2 by Sub-20 fs Photoelectron Imaging Using 159 nm Probe Pulses. *J. Chem. Phys.* **2015**, *142*, No. 074308.

(19) Horio, T.; Spesyvtsev, R.; Furumido, Y.; Suzuki, T. Real-Time Detection of $S(^1D_2)$ Photofragments Produced from the $^1B_2(^1\Sigma_u^+)$ State of CS_2 by Vacuum Ultraviolet Photoelectron Imaging Using 133 nm Probe Pulses. *J. Chem. Phys.* **2017**, *147*, No. 013932.

(20) Smith, A. D.; Warne, E. M.; Bellshaw, D.; Horke, D. A.; Tudorovskya, M.; Springate, E.; Jones, A. J. H.; Cacho, C.; Chapman, R. T.; Kirrander, A.; Minns, R. S. Mapping the Complete Reaction Path of a Complex Photochemical Reaction. *Phys. Rev. Lett.* **2018**, *120*, 18303.

(21) Warne, E. M.; Smith, A. D.; Horke, D. A.; Springate, E.; Jones, A. J. H.; Cacho, C.; Chapman, R. T.; Minns, R. S. Time Resolved Detection of the $S(^1D)$ Product of the UV Induced Dissociation of CS_2. *J. Chem. Phys.* **2021**, *154*, No. 034302.

(22) Trabelsi, T.; Al-Mogren, M. M.; Hochlaf, M.; Francisco, J. S. Mechanistic Study of the Photoexcitation, Photoconversion, and Photodissociation of CS_2. *J. Chem. Phys.* **2018**, *149*, No. 064304.

(23) Oliveira, A. P.; Jalbert, G.; Rocha, A. B. Generalized Oscillator Strengths of Carbon Disulfide Calculated by Multireference Configuration Interaction. *J. Chem. Phys.* **2019**, *150*, 174116.

(24) Li, Z. X.; Zhao, M.; Xie, T.; Chang, Y.; Luo, Z. J.; Chen, Z. C.; Wang, X. G.; Yuan, K. J.; Yang, X. M. Velocity Map Imaging Studies of the Photodissociation of CS_2 by Two-Photon Excitation at around 303−315 nm. *Mol. Phys.* **2021**, *119*, No. e1813911.

(25) Hochlaf, M. Ab Initio Investigations of the Unimolecular Decay of CS_2^+ for Internal Energies Lower Than 10 eV. *J. Phys. B: At., Mol. Opt. Phys.* **2004**, *37*, 595−608.

(26) Fuji, T.; Horio, T.; Suzuki, T. Generation of 12 fs Deep-Ultraviolet Pulses by Four-Wave Mixing through Filamentation in Neon Gas. *Opt. Lett.* **2007**, *32*, 2481−2483.

(27) Horio, T.; Spesyvtsev, R.; Suzuki, T. Simultaneous Generation of Sub-20 fs Deep and Vacuum Ultraviolet Pulses in a Single Filamentation Cell and Application to Time-Resolved Photoelectron Imaging. *Opt. Express* **2013**, *21*, 22423−22428.

(28) Horio, T.; Spesyvtsev, R.; Suzuki, T. Generation of Sub-17 fs Vacuum Ultraviolet Pulses at 133 nm Using Cascaded Four-Wave Mixing through Filamentation in Ne. *Opt. Lett.* **2014**, *39*, 6021−6024.

(29) Karashima, S.; Humeniuk, A.; Uenishi, R.; Horio, T.; Kanno, M.; Ohta, T.; Nishitani, J.; Mitrić, R.; Suzuki, T. Ultrafast Ring-Opening Reaction of 1,3-Cyclohexadiene: Identification of Non-adiabatic Pathway via Doubly Excited State. Submitted for publication, 2021.

(30) Corkum, P. B. Plasma Perspective on Strong-Field Multiphoton Ionization. *Phys. Rev. Lett.* **1993**, *71*, 1994−1997.

(31) Krause, J. L.; Schafer, K. J.; Kulander, K. C. High-Order Harmonic-Generation from Atoms and Ions in the High-Intensity Regime. *Phys. Rev. Lett.* **1992**, *68*, 3535−3538.

(32) Lewenstein, M.; Balcou, P.; Ivanov, M. Y.; L'Huillier, A.; Corkum, P. B. Theory of High-Harmonic Generation by Low-Frequency Laser Fields. *Phys. Rev. A: At., Mol., Opt. Phys.* **1994**, *49*, 2117−2132.

(33) Grebenshchikov, S. Y. Private Communication.

(34) Hemley, R. J.; Leopold, D. G.; Roebber, J. L.; Vaida, V. The Direct Ultraviolet Absorption Spectrum of the $^1\Sigma_g^+ \rightarrow {}^1B_2(^1\Sigma_u^+)$ Transition of Jet-Cooled CS_2. *J. Chem. Phys.* **1983**, *79*, 5219−5227.

(35) Roebber, J. L.; Vaida, V. The Direct Ultraviolet Absorption Spectrum of the $^1\Sigma_g^+ \rightarrow {}^1B_2(^1\Sigma_u^+)$ Transition of Jet-Cooled $^{13}C^{32}S_2$ and $^{12}C^{34}S_2$. *J. Chem. Phys.* **1985**, *83*, 2748−2753.

(36) Martin, W. C.; Zalubas, R.; Musgrove, A. Energy Levels of Sulfur, S I through S XVI. *J. Phys. Chem. Ref. Data* **1990**, *19*, 821−880.

(37) Zuin, L.; Innocenti, F.; Costa, M. L.; Dias, A. A.; Morris, A.; Paiva, A. C. S.; Stranges, S.; West, J. B.; Dyke, J. M. An Initial Investigation of S and SH with Angle Resolved Photoelectron

Spectroscopy Using Synchrotron Radiation. *Chem. Phys.* **2004**, *298*, 213−222.
(38) Barthel, M.; Flesch, R.; Rühl, E.; McLaughlin, B. M. Photoionization of the $3s^2\ 3p^4\ ^3P$ and the $3s^2\ 3p^4\ ^1D$, ^1S States of Sulfur: Experiment and Theory. *Phys. Rev. A: At., Mol., Opt. Phys.* **2015**, *91*, 013406.
(39) Moltzen, E. K.; Klabunde, K. J.; Senning, A. Carbon Monosulfide: A Review. *Chem. Rev.* **1988**, *88*, 391−406.
(40) Bergeman, T.; Cossart, D. The Lower Excited-States of CS: A Study of Extensive Spin-Orbit Perturbations. *J. Mol. Spectrosc.* **1981**, *87*, 119−195.
(41) Gauyacq, D.; Horani, M. The Electronic Spectrum of the CS^+ Molecular Ion: Rotational Analysis and Perturbation Effects in the $A^2\Pi$ - $X^2\Sigma^+$ Transition. *Can. J. Phys.* **1978**, *56*, 587−600.
(42) Honjou, N. Ab Initio Study of Molecular Vibrations in the $X^2\Sigma^+$, $A^2\Pi$, $B^2\Sigma^+$ and $C^2\Sigma^+$ States of CS^+ and the Vibrational Structure in the Photoelectron Spectrum of CS. *Chem. Phys.* **2008**, *344*, 128−134.
(43) Kruit, P.; Read, F. H. Magnetic-Field Parallelizer for 2π Electronspectrometer and Electron-Image Magnifier. *J. Phys. E: Sci. Instrum.* **1983**, *16*, 313−324.

https://doi.org/10.1021/acs.jpclett.1c00864
J. Phys. Chem. Lett. 2021, 12, 3755−3761